

# Constraints on the abundance of primordial black holes from lensing of gravitational waves for the third-generation gravitational wave detector

Huan Zhou,<sup>1</sup> Zhengxiang Li,<sup>2\*</sup> Kai Liao,<sup>3</sup> and Zhiqi Huang<sup>1</sup>

<sup>1</sup>*School of Physics and Astronomy, Sun Yat-sen University, Zhuhai, 519082, China*

<sup>2</sup>*Department of Astronomy, Beijing Normal University, Beijing 100875, China*

<sup>3</sup>*School of Physics and Technology, Wuhan University, Wuhan 430072, China*

Accepted XXX. Received YYY; in original form ZZZ

## ABSTRACT

Since the first gravitational wave (GW) event from binary black hole (BBH) was detected by LIGO-Virgo, GWs have become a useful probe on astrophysics and cosmology. If primordial black holes (PBHs) contribute a significant fraction of dark matter at wide mass range, they will cause microlensing in the GW signals with long wavelengths that are distinct from the lensing effects of electromagnetic signals from astrophysical objects. In this paper, we apply the lensing effect of GW from BBH to derive constraints on the abundance of PBHs for the Cosmic Explorer, a third-generation ground-based GW detector. We firstly consider two channels of formation of BBH that contribute to low and high redshift GW sources, including the astrophysical origin BBH scenario, and the primordial origin BBH scenario. Secondly, comparing with the method of optical depth, we use the Bayesian analysis to derive constraints on the abundance of PBHs with different mass function of lens taken into consideration. For a null search with 1000 detected GW events of BBH, we find that the abundance of PBHs could be constrained to  $\leq 0.1\%$  in the mass range  $\geq 500 M_{\odot}$  at 68% confidence level. In addition, if a GW event lensed by  $M_{\text{PBH}} = 100 - 300 M_{\odot}$  is detected in 100 detected GW events of BBH, we can derive that the abundance of PBHs is from 2.3% to 25.2% in this mass range with the Bayesian analysis.

**Key words:** dark matter, gravitational lensing; micro, gravitational waves

## 1 INTRODUCTION

The first detection of gravitational wave (GW) event from binary black hole (BBH) merger opened a new window in astronomy (Abbott et al. 2016). GWs have been proposed as very powerful probes of astrophysics and cosmology, such as solving Hubble tension (Hotokezaka et al. 2019; Feeney et al. 2021), constraining the speed of GWs (Abbott et al. 2017), and constraints on the dark matter candidates (Yoshida & Soda. 2018; Basak et al. 2022). With the increasing sensitivity of the current and future detectors, such as Einstein Telescope (ET) (Reitze et al. 2019), Cosmic Explorer (CE) (Reitze et al. 2019), Laser Interferometer Space Antenna (LISA) (Amaro-Seoane et al. 2017), Taiji (Hu & Wu. 2017), Tianqin (Luo et al. 2016), and DECihertz Interferometer Gravitational wave Observatory (DECIGO) (Kawamura et al. 2019), the increasingly detectable GW events and multiband GW observations are expected to solve these open questions in modern astrophysics and cosmology.

Dark matter (DM) makes up about one quarter of the total energy budget of the universe, which is consistent with many popular cosmological observations. However, we still know

little about the constituent of DM, especially in small scales. Primordial black holes (PBH) is a theoretical DM candidate which have been a field of great astrophysical interest. In principle, the mass of PBHs can range from the Planck mass to the level of the black hole in the centre of the galaxy. Therefore, numerous methods have been proposed to constrain the fraction of PBHs in DM  $f_{\text{PBH}} = \Omega_{\text{PBH}}/\Omega_{\text{DM}}$  at present universe in various possible mass windows. (See Sasaki et al. (2018); Green & Kavanagh (2021); Carr et al. (2021) for recent reviews.) Gravitational lensing effect is a powerful probe to constrain the abundance of PBHs over a broad mass range from  $\mathcal{O}(10^{-10} M_{\odot})$  to  $\mathcal{O}(10^{10} M_{\odot})$ . For example, observing a large number of stars and looking for amplifications in their brightness caused by lensing effect of intervening massive objects could yield constraints on the abundance of deflectors (Alcock et al. 2001; Tisserand et al. 2007; Griest et al. 2013; Niikura et al. 2019a,b). Searching lensing systems that observed signals of transient sources like the fast radio bursts (FRBs) or gamma ray bursts (GRBs) would appear echoes were proposed to put constraints on the compact dark matter (Muñoz et al. 2016; Ji et al. 2018; Laha et al. 2020; Liao et al. 2020b; Zhou et al. 2022a,b; Lin et al. 2022). Searching multiple images produced by milli-lensing of possible persistent sources like the compact radio sources (CRSS) is another

\* E-mail: zxli918@bnu.edu.cn

powerful probe (Kassiola et al. 1991; Wilkinson et al. 2001; Zhou et al. 2022c). Similar to electromagnetic waves, GWs can also be lensed by compact dark matter. However, the most significant difference when looking for the lensing of GWs from compact object binaries instead of lensing of stellar light is that the characteristic wavelength of GW signals is very long and wave optics effect become important. Therefore, we should consider the diffraction effect in the lensing of GW, which distorts the GW waveform as the fringes. Jung & Shin. (2019) first proposed that the lensing effect of GWs observed by advanced LIGO can probe the compact dark matter. There are many subsequent studies using the lensing effect of GW have been performed (Liao et al. 2020a; Urrutia & Vaskonen 2021; Wang et al. 2021; Basak et al. 2022). Especially in Basak et al. (2022) work, they constrain the fraction of compact dark matter in the mass range  $10^2 - 10^5 M_\odot$  to be less than 50% – 80% from the non-detection of microlensing signals in currently available BBH events detected by LIGO-Virgo. This result is still weaker compared with the results of other methods (Sasaki et al. 2018; Green & Kavanagh 2021; Carr et al. 2021).

In this paper, based on GW events that mainly consist of signals from the coalescence of BBH, we study the ability of the Cosmic Explorer (CE), a future third-generation ground-based GW detector, to constrain the abundance of PBHs through gravitational lensing of GW signals from BBH<sup>1</sup>. It should be noted that, there are two most important differences between our analyses and previous works (Jung & Shin. 2019; Liao et al. 2020a; Urrutia & Vaskonen 2021; Wang et al. 2021). Firstly, there are still many discussions about the origin mechanism of GWs of BBH. Therefore, we assume two channels of formation of BBH, including astrophysical and primordial origins, which correspond to different redshift and mass distribution of GW sources. Secondly, based on Basak et al. (2022), we compare the constraints of the abundance of PBHs from the Bayesian analysis with the results from the method of optical depth. Moreover, previous works are based on the monochromatic mass distribution of lens, here we add the extended mass distribution of lens into the method of Bayesian analysis to constrain the PBHs.

This paper is organized as follows: In Section 2, we introduce the lensing effect of GW with wave optical description; In Section 3, we firstly give our simulated models, the primordial origin BBH model and the astrophysical origin BBH model. Then we introduce the method of Bayesian analysis. The results of constraints are presented in Section 4. Finally, we summarize our conclusions in Section 5. Throughout, we use the concordance  $\Lambda$ CDM cosmology with the best-fitting parameters from the recent *Planck* observations (Planck Collaboration, 2020), and the natural units of  $G = c = 1$  in all equations.

<sup>1</sup> For the third generation ground-based GW detectors, the sensitivities of ET and CE are approximately the same, which determines their abilities to constrain the abundance of PBHs are similar. Therefore, we only use CE as the representative of the third generation ground-based GW detectors.

## 2 LENSING OF GRAVITATIONAL WAVE

In this Section, we briefly review the theory of lensing of GWs described by the wave optics limit (Takahashi & Nakamura. 2003). A GW is described by a tiny perturbation  $h_{\mu\nu}$  over the background metric  $g_{\mu\nu}$ . The amplitude  $h$  of the perturbation  $h_{\mu\nu}$  follows the equation as

$$\partial(\sqrt{-g}g^{\mu\nu}\partial_\nu h) = 0. \quad (1)$$

Based on the lensing events occurring near the deflector, the equation of lensing GW can be approximated in the Fourier space as

$$(\Delta + 4\pi^2 f^2)\bar{h} = 16\pi^2 f^2 U \bar{h}, \quad (2)$$

where  $U$  is the lensing potential in the background metric  $g_{\mu\nu}$ , and  $\bar{h}$  is Fourier transform of  $h$ . We can define the dimensionless amplification factor as

$$F(f) = \frac{\bar{h}^L(f)}{\bar{h}_0(f)}, \quad (3)$$

where  $\bar{h}^L(f)$  and  $\bar{h}_0(f)$  correspond to lensed and unlensed ( $U = 0$ ) signal, respectively. For the unlensed waveform  $\bar{h}_0(f)$  from BBHs merger event, we ignore higher order post-Newtonian terms for simplicity (Jung & Shin. 2019; Liao et al. 2020a),

$$\bar{h}_0(f) = \sqrt{\frac{5}{24}} \frac{\mathcal{M}_z^{5/6} \mathcal{F}}{\pi^{2/3} d_L(z)} f^{-7/6} \exp\{i[\Psi(f) + \Psi_0]\}, \quad (4)$$

where

$$\Psi(f) = 2\pi f t_c + \frac{3}{128} (\pi \mathcal{M}_z f)^{-5/3}, \quad (5)$$

$\mathcal{M}_z$ ,  $t_c$  and  $d_L$  represent the redshifted chirp mass, coalescence time and luminosity distance, respectively.  $\mathcal{F}$  is the angular orientation function which contains all angle dependence of the detector response to GW events, and we give a distribution for  $\mathcal{F}$  (Finn. 1996)

$$P(\mathcal{F}) = 20\mathcal{F}(1 - \mathcal{F})^3 \mathcal{H}(\mathcal{F}) \mathcal{H}(1 - \mathcal{F}), \quad (6)$$

where  $\mathcal{H}$  is the Heaviside step function. The solution of Equation (3) in the thin lens approximation is given by

$$F(f) = \frac{D_s D_1 \theta_E^2 (1 + z_1) f}{D_{ls} i} \int d^2x \exp[2\pi i f t_d(\vec{x}, \vec{y})], \quad (7)$$

where  $D_s$ ,  $D_1$  and  $D_{ls}$  represent the angular diameter distance to the source, to the lens, and between the source and the lens, respectively. In addition,  $\theta_E$  is Einstein radius,  $t_d$  is the arrival time delay of the wave to the observer

$$t_d(\vec{x}, \vec{y}) = \frac{D_s D_1 \theta_E^2 (1 + z_1)}{D_{ls}} \left[ \frac{1}{2} |\vec{x} - \vec{y}|^2 - \psi(\vec{x}) + \phi_m(\vec{y}) \right], \quad (8)$$

where  $\psi(\vec{x})$  is dimensionless deflection potential and  $\phi_m(\vec{y})$  is chosen such that the minimum arrival time delay is zero. For a point mass lens, potential  $\psi(\vec{x}) = \ln x$  and  $\phi_m(\vec{y}) = 0.5(x_m - y)^2 - \ln x_m$  with  $x_m = 0.5(y + \sqrt{y^2 + 4})$ . In this case,  $F(f)$  can be written as

$$F(f) = \exp \left[ \frac{\pi\omega}{4} + i\frac{\omega}{2} \left( \ln \frac{\omega}{2} - 2\phi_m(y) \right) \right] \times \Gamma \left( 1 - \frac{i\omega}{2} \right) {}_1F_1 \left( \frac{i\omega}{2}, 1, \frac{i\omega y^2}{2} \right), \quad (9)$$

where  $\omega = 8\pi M_{\text{PBH}}(1 + z_1)f$  is a dimensionless parameter and  ${}_1F_1$  is the confluent hypergeometric function. For a point

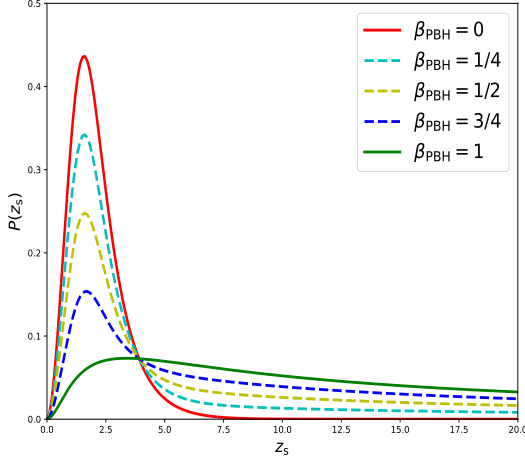


**Figure 1.** Redshift distribution of GW events of BBH with different  $\beta_{\text{PBH}}$ .

mass lens, the dimensionless amplification factor  $F(f)$  depends only on the redshifted mass of lens  $M_1^z \equiv (1+z_1)M_{\text{PBH}}$  and the source position  $y$ .

### 3 METHODOLOGY

In this Section, we introduce the simulation of GWs and specify the Bayesian analysis.

#### 3.1 Simulation

Understanding the origin of GWs of BBHs is an essential scientific goal and is still an open issue. There are two explanations for observed BBH events, i.e. the PBH binary model and the astrophysical black hole (ABH) binary model.

For PBH binaries, PBHs formed in the early universe from gravitational collapse of primordial density perturbations (Sasaki et al. 2018; Green & Kavanagh 2021; Carr et al. 2021), and have quite different evolutionary histories than ABHs which originate from the demise of massive stars. There are two distinct formation mechanisms of PBH binaries which form at different epoch in the cosmic history. The first mechanism of PBH binaries operates by decoupling from the cosmic expansion in the universe dominated by radiation (Sasaki et al. 2016; Ali-Haïmoud, & Kamionkowski 2017; Chen & Huang 2018; Raidal et al. 2017, 2018). The second mechanism is that PBHs binaries form in the late universe by the close encounter (Sasaki et al. 2016; Raidal et al. 2017). Comparing with the second formation mechanism of PBH binaries, the mergers of PBH binaries from the first formation mechanism contributes dominant GW sources of BBHs (Sasaki et al. 2016; Raidal et al. 2017). Therefore, as suggested in Ali-Haïmoud, & Kamionkowski (2017); Chen & Huang (2018); Raidal et al. (2017, 2018), we mainly consider the first formation mechanism of PBH binaries, and the comoving merger rate density in units of  $\text{Gpc}^{-3}\text{yr}^{-1}$  is given as

$$R_{\text{PBH}}(z) = R_0 \left( \frac{t(z)}{t_0} \right)^{-\frac{34}{37}} \quad (10)$$

where  $R_0$  and  $t_0$  represent the  $R_{\text{PBH}}(z=0)$  and the current age of the universe, respectively. Based on the merger rate, we can obtain the normalized redshift distribution of PBH binaries as

$$P_{\text{PBH}}(z) = \frac{1}{Z_{\text{PBH}}} \frac{R_{\text{PBH}}(z)}{1+z} \frac{dV_c}{dz}, \quad (11)$$

where  $Z_{\text{PBH}}$  is the normalization constant and  $dV_c/dz$  is the differential comoving volume. The term  $1+z$  accounts for the cosmological time dilation. Since we still do not understand the detailed process of PBH formation, we first assume that PBH mass distribution in PBH binaries is described by the following model-independent log-normal mass function

$$P_{\text{PBH}}(m) = \frac{1}{\sqrt{2\pi}\sigma m} \exp\left(-\frac{\ln^2(m/m_c)}{2\sigma^2}\right), \quad (12)$$

where  $m_c$  and  $\sigma$  denote the peak mass of  $mP(m)$  and the width of mass spectrum, respectively. This model-independent parameterization is often a good approximation if PBHs produced from a smooth symmetric peak in the inflationary power spectrum (Green 2016; Kannike et al. 2017), and is often used in the literature to derive constraints on the PBH from GW measurements detected by the LIGO-Virgo (Chen et al. 2019; Wu 2020; De Luca et al. 2020; Hütsi, et al. 2021; Wong et al. 2021).

For ABH binaries, we follow the widely accepted ‘‘Vangioni’’ model to estimate the comoving merger rate (Dvorkin et al. 2016), which is a convolution of the birthrate of ABHs  $R_b(t(z)-t, m)$  with the distribution of the time delays  $P(t)$  between the formation and merger

$$R_{\text{ABH}}(z) = \int_{>1M_\odot} \int_{t_{\min}}^{t_{\max}} R_b(t(z)-t, m) \times P(t) dt dm, \quad (13)$$

where  $t_{\min} = 50$  Myr, and  $t_{\max}$  is set to the Hubble time. In addition,  $R_b(t, m)$  can be estimated by (Dvorkin et al. 2016)

$$R_b(t, m) = \int \psi[t - \tau(m')] \phi(m') \delta(m - g_b^{-1}(m_{\text{bh}})) dm', \quad (14)$$

where  $m_{\text{bh}}$  is the mass of the remnant black hole,  $\tau(m)$  is the lifetime of a progenitor star and  $\phi(m)$  is the initial mass function. The star formation rate  $\psi(t)$  in  $R_b(t, m)$  is given by

$$\psi(z) = k \frac{a \exp[b(z - z_m)]}{a - b + b \exp[a(z - z_m)]}, \quad (15)$$

where the parameter set  $\{k, a, b, z_m\}$  is from the Fiducial model  $\{0.178 M_\odot \text{yr}^{-1} \text{Mpc}^{-3}, 2.37, 1.80, 2.00\}$  given in Vangioni et al. (2015), which corresponds to the classical isolated binary evolution of ABH binaries model. Similar to the PBH binaries, the redshift distribution of ABH binaries can be given as

$$P_{\text{ABH}}(z) = \frac{1}{Z_{\text{ABH}}} \frac{R_{\text{ABH}}(z)}{1+z} \frac{dV_c}{dz}, \quad (16)$$

where  $Z_{\text{ABH}}$  is the normalization constant. We use a power law mass distribution for the heavier black hole in the ABH binaries as (Liao et al. 2020a; Basak et al. 2022)

$$P_{\text{ABH}}(m) = \frac{1}{Z_m} m^{-2.35} \mathcal{H}(m - 5 M_\odot) \mathcal{H}(100 M_\odot - m), \quad (17)$$

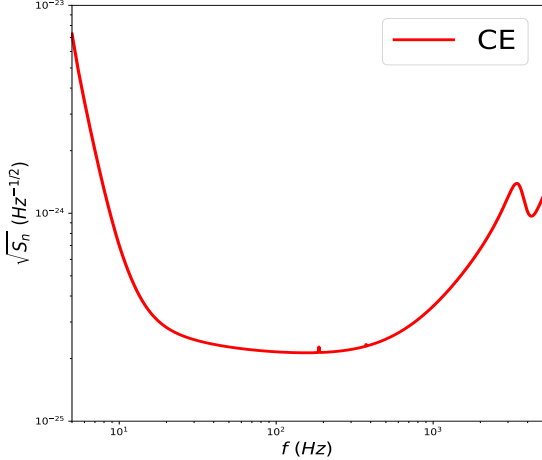


**Figure 2.** The sensitivity curve of the third-generation gravitational wave detector, i.e. the Cosmic Explorer.

where  $Z_m$  is the normalization constant.

Next, we consider the redshift distribution of simulated GW events of BBH include both PBH and ABH populations

$$P(z) = \beta_{\text{PBH}} P_{\text{PBH}}(z) + (1 - \beta_{\text{PBH}}) P_{\text{ABH}}(z), \quad (18)$$

where  $\beta_{\text{PBH}}$  is the fraction of the PBH merger rate to the total merger rate. As shown in Figure 1, when  $\beta_{\text{PBH}} = 0$  and  $\beta_{\text{PBH}} = 1$ , the redshift distribution of GW events of BBH recovers to  $P_{\text{ABH}}(z)$  and  $P_{\text{PBH}}(z)$ , respectively. In particular, the contribution to the number of BBH events from high redshift ( $z > 7$ ) for ABH binaries model can be negligible compared with the PBH binaries model. In the following analysis, we only take the  $\beta_{\text{PBH}} = 0, 0.5, 1$  for the sake of comparison. For the mass distribution of BBHs, we take  $(m_c, \sigma) = (30 M_\odot, 0.3)$  as Ng Ken et al. (2022) work in the PBH binaries, which encompasses the most sensitive mass range of the next-generation GW detectors and can account for the current GW data as presented in Chen et al. (2019); Wu (2020); De Luca et al. (2020); Hütsi, et al. (2021); Wong et al. (2021). For the mass distribution of ABH binaries, we assume that the mass of black hole is in the range of  $5 M_\odot \leq m_2 < m_1 \leq 100 M_\odot$ . The heavier black hole  $m_1$  satisfies the mass distribution as equation (17), and the mass of  $m_2$  uniformly distributes in the interval  $[5 M_\odot, m_1]$ .

### 3.2 Bayesian analysis

Following the method presented in Basak et al. (2022), we introduce the posterior distribution that the mass of PBH lens is larger than  $50 M_\odot$  to constrain on the  $f_{\text{PBH}}$ . We assume that the number of detected GW events of BBH ( $N$ ) follow a Poisson distribution with mean  $\Lambda$ , whose posterior distribution can be estimated as

$$p(\Lambda|N) = \frac{1}{Z} p(\Lambda) p(N|\Lambda), \quad (19)$$

where  $Z$  is the normalization constant.  $p(\Lambda)$  is the flat prior distribution for  $\Lambda$

$$p(\Lambda) = \frac{1}{\Lambda^{\text{max}}} \mathcal{H}(\Lambda) \mathcal{H}(\Lambda^{\text{max}} - \Lambda), \quad (20)$$

where  $\Lambda^{\text{max}}$  is maximum possible values of  $\Lambda$ . The likelihood  $p(N|\Lambda)$  is approximated by a Poisson distribution

$$p(N|\Lambda) = \frac{\Lambda^N \exp(-\Lambda)}{N!}. \quad (21)$$

Similarly, from the lensed observations ( $N_1$ ), the posterior on the Poisson mean  $\Lambda_1$  of the number for lensed events can be calculated as

$$p(\Lambda_1|N_1) = \frac{1}{Z_1} p_1(\Lambda_1) p_1(N_1|\Lambda_1), \quad (22)$$

where  $Z_1$  is the normalization factor. we also take  $p_1(\Lambda_1)$  as the flat prior distribution for  $\Lambda_1$

$$p_1(\Lambda_1) = \frac{1}{\Lambda_1^{\text{max}}} \mathcal{H}(\Lambda_1) \mathcal{H}(\Lambda_1^{\text{max}} - \Lambda_1), \quad (23)$$

where  $\Lambda_1^{\text{max}}$  is the largest value that corresponds to the situation of  $f_{\text{PBH}} = 1$  following the equation (A1) in Basak et al. (2022). The likelihood  $p(N_1|\Lambda_1)$  is

$$p(N_1|\Lambda_1) = \frac{\Lambda_1^{N_1} \exp(-\Lambda_1)}{N_1!}. \quad (24)$$

To calculate the posterior on the fraction of lensed events  $u \equiv \Lambda_1/\Lambda$ , we can use the ratio distribution assuming the  $\Lambda$  and  $\Lambda_1$  are independent to get

$$p(u|\{N, N_1\}) = \frac{1}{Z_u} \int_0^{+\infty} \Lambda p(\Lambda|N) p(u\Lambda|N_1) d\Lambda, \quad (25)$$

where  $Z_u$  is normalization constant that determined by  $\int_0^{u^{\text{max}}} p(u|\{N, N_1\}) du = 1$ , where  $u^{\text{max}}$  is maximum value of  $u$  (corresponding to  $f_{\text{PBH}} = 1$ ). Finally, the posterior of  $f_{\text{PBH}}$  can be written as

$$p(f_{\text{PBH}}|\{N, N_1\}) = \frac{1}{Z_{f_{\text{PBH}}}} p(u|\{N, N_1\}) \left| \frac{du}{df_{\text{PBH}}} \right|, \quad (26)$$

where  $Z_{f_{\text{PBH}}}$  is normalization constant and  $\left| \frac{du}{df_{\text{PBH}}} \right|$  is the Jacobian determinant. We determine this Jacobian determinant as these steps:

- **Generating the detectable BBH events:** Based on the redshift distribution and mass distribution in Simulation subsection, we can simulate  $\mathcal{O}(10^4)$  detectable unlensed BBH events with signal-to-noise ratio ( $\text{SNR} \geq 8$ ) for CE. SNR of unlensed GW can be computed as

$$\text{SNR} = \sqrt{4 \int_{f_0}^{f_1} \frac{|\bar{h}_0(f)|^2}{S_n(f)} df}, \quad (27)$$

where the lower cutoff  $f_0$  depends on the sensitivity curve  $\sqrt{S_n(f)}$  of CE <sup>2</sup> as shown in Figure 2, and we adopt  $f_0 = 5$  Hz. The cutoff frequency  $f_1$  is adopted by the value  $\min\{[3\sqrt{3}\pi(1+z_s)(m_1+m_2)]^{-1}, 5 \text{ kHz}\}$ .

<sup>2</sup> Sensitivity curve of CE is available via <https://cosmicexplorer.org/sensitivity.html>

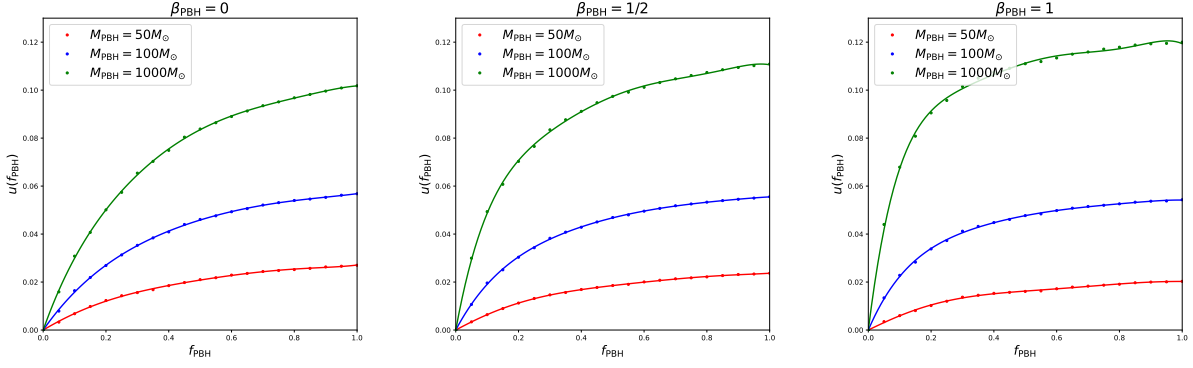


**Figure 3.** The fraction of simulated events as the process in Section 3.2, shown as a function of  $f_{\text{PBH}}$ . The left, middle and right subfigures correspond to different  $\beta_{\text{PBH}}$ . In each subfigure, different colors correspond to different lens masses. The curves are power series polynomial fits.

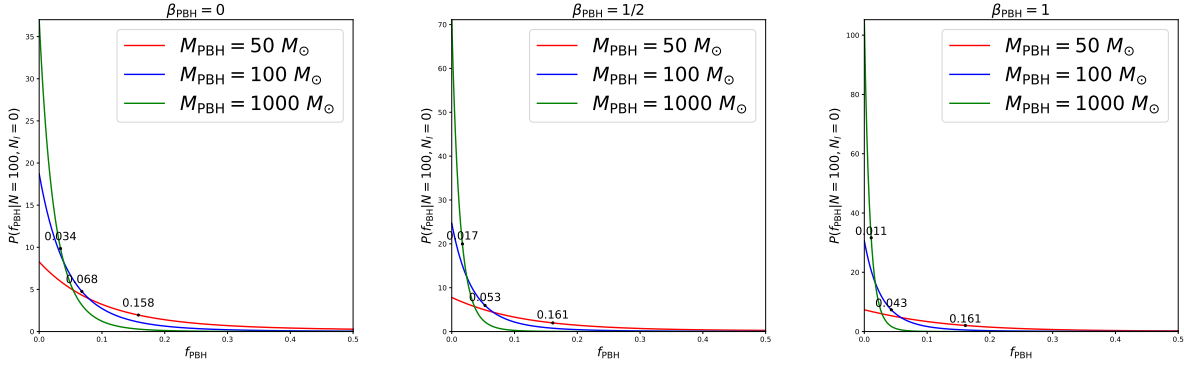


**Figure 4.** Posteriors on  $f_{\text{PBH}}$  obtained from the non-observation of microlensing signals  $N_l = 0$  in the 100 BBHs events detected by CE. The same as Figure 3, the left, middle and right correspond to different  $\beta_{\text{PBH}}$ , and curves with different color correspond to different lens masses. The 68% credible upper limits are shown by dots.

- **Generating the lensed GW events:** By assuming that the PBHs are distributed uniformly in comoving volume, the probability that a GW event located at  $z_s$  is lensed by an intervening PBH can be given by  $P_l(z_s) = 1 - \exp(-\tau(z_s))$ . We identify a BBH GW signal as a lensed event when  $P_l(z_s)$  is larger than a random number uniformly distribution between 0 and 1.  $\tau(z_s)$  is the optical depth at  $z_s$

$$\tau(z_s) = \int_0^{z_s} \tau(z_1, z_s) dz_1, \quad (28)$$

where  $\tau(z_s, z_1)$  is the differential optical depth given by

$$\tau(z_s, z_1) = \frac{3}{2} f_{\text{PBH}} y_0^2 \Omega_{\text{DM}} \frac{H_0^2 (1+z_1)^2}{H(z_1)} \frac{D_l D_{ls}}{D_s}. \quad (29)$$

When a GW event is identify as lensed event, the  $z_1$  is adopted from a probability distribution given by equation (29). The impact parameter  $y$  is drawn from the distribution  $P(y) \propto y$  in the range of  $y \in [0, 5]$ .

- **Identifying BBH events with wave optics effect:** The time delay caused by a point mass is given by

$$\Delta t_{\text{lensing}} = 4M_l^z \left[ \frac{y\sqrt{y^2+4}}{2} + \ln \left( \frac{\sqrt{y^2+4}+y}{\sqrt{y^2+4}-y} \right) \right], \quad (30)$$

The duration of GW signal can be approximated as

$$t_{\text{signal}} = \frac{5}{256} \mathcal{M}_s^{-5/3} (\pi f_0)^{-8/3} + 10^4 M_s^z, \quad (31)$$

where  $\mathcal{M}_s^z$  and  $M_s^z$  are redshifted chirp mass and total mass of BBH, respectively. We consider those lensed signals with  $\Delta t_{\text{lensing}} \leq t_{\text{signal}}$  satisfy wave optics effects.

- **Computing lensed criterion:** After generating unlensed and lensed gravitational waveform with simulated source and lens parameters, we use the test SNR as criterion following Jung & Shin. (2019); Liao et al. (2020a)

$$\text{SNR}_{\text{test}} = \sqrt{4 \int_{f_0}^{f_1} \frac{|\bar{h}^L(f) - \bar{h}_{\text{best-fit}}(f)|^2}{S_n(f)} df}. \quad (32)$$

To ensure that the difference between the lensed GW signal and the unlensed signal is significant enough, which leads to figure out the lensing signal, we adopt  $\text{SNR}_{\text{test}} \geq 8$  as the lensed criterion. In addition, we use the standard template to fit the lensed signal by varying the amplitude and phase.

- **Calculating  $u(f_{\text{PBH}})$ :** We can obtain  $u(f_{\text{PBH}})$

$$u(f_{\text{PBH}}) = \frac{N_{\text{lensed}}(f_{\text{PBH}})}{N_t}, \quad (33)$$

where  $N_{\text{lensed}}$  and  $N_t$  represent the number of lensed events

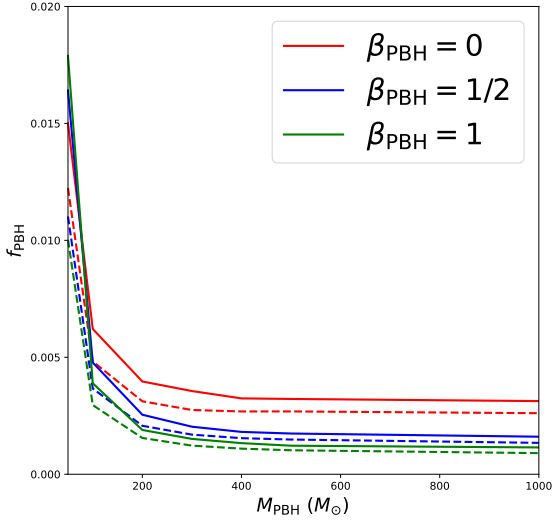


**Figure 5.** Constraints on the upper limits of fraction of dark matter in the form of PBHs at 68% confidence level, shown as a function of lens mass with 1000 observed BBH events. Lines with different color correspond to results with different  $\beta_{\text{PBH}}$ . Solid and dashed lines represent the upper limits using the Bayesian analysis and the optical depth, respectively.

expected to be detected and total number of detectable events, respectively. If we take the mass of lens  $M_{\text{PBH}}$  as a constant,  $u(f_{\text{PBH}})$  corresponds to the fraction of simulated events for the monochromatic mass distribution of lens. Here we also take a tested mass function for the lens with the power-law form

$$P_1(M_{\text{PBH}}) = \mathcal{N}_{\text{pl}} M_{\text{PBH}}^{\gamma-1} \mathcal{H}(M_{\text{PBH}} - 10 M_{\odot}) \mathcal{H}(1000 M_{\odot} - M_{\text{PBH}}), \quad (34)$$

where  $\mathcal{N}_{\text{pl}}$  is the normalization constant, and the exponent of the power law is denoted by  $\gamma$ .

Then we can obtain the limit of  $f_{\text{PBH}}$  from the posterior distribution following Equation (26).

For comparing with the Bayesian analysis method, we also use the optical depth method in our results. For this method, we can use Equation (32) to obtain the maximum impact parameter  $y_{\text{max}}$ , and then calculate the cross section of PBH

$$\sigma(M_{\text{PBH}}, z_s, z_l) = 4\pi M_{\text{PBH}} \frac{D_l D_{\text{ls}}}{D_s} y_{\text{max}}^2. \quad (35)$$

By using the cross section to calculate the optical depth  $\tau_i$  for each GW event, we can obtain the expected number of lensed events (Liao et al. 2020a)

$$N_{\text{lensed}}(M_{\text{PBH}}, f_{\text{PBH}}) = \sum_{i=1}^{N_{\text{total}}} \tau_i. \quad (36)$$

For a null search of lensed GW signals, then the constraint on the upper limit of the fraction of DM in the form of PBHs can be estimated.

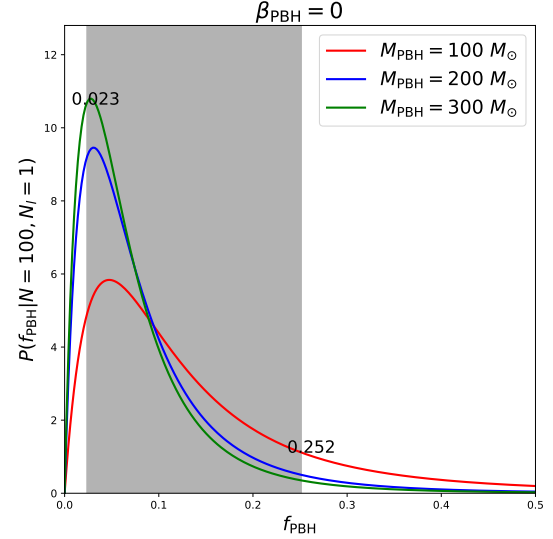


**Figure 6.** Similar as Figure 4, posteriors on  $f_{\text{PBH}}$  obtained from an identification of microlensing signals  $N_l = 1$  in the 100 BBHs events detected by CE. Lines with different color correspond to results with different different lens masses. The shadow represents the range of  $f_{\text{PBH}}$  with the redshift of source being 2 and the redshifted lens mass being  $300 M_{\odot}$ .

## 4 RESULTS

We consider two formation channels of BBHs, i.e. the ABH binary scenario and the PBH binary scenario, to contribute the low and high redshift GW events with a parameterized fraction  $\beta_{\text{PBH}}$ . For the monochromatic mass distribution of lens mass, the fraction of simulated events with  $\text{SNR}_{\text{test}} \geq 8$  is shown as a function of  $f_{\text{PBH}}$  in Figure 3. This enables us to calculate the posterior of  $f_{\text{PBH}}$ . Firstly, Figure 4 shows the posterior of  $f_{\text{PBH}}$  assuming 100 observed BBH events without lensed signal identification. The 68% upper limits are shown as black dots in each subfigure of Figure 4. We find that  $\beta_{\text{PBH}}$  is larger (more high redshift GW events of BBH), the constraints on  $f_{\text{PBH}}$  are stronger. However, there is no significant improvement of these constraints. In Figure 5, we show the constraints of  $f_{\text{PBH}}$  from the detection of 1000 BBH events without lensed signal identification by using the Bayesian analysis and the optical depth respectively. The magnitude of results obtained by these two methods are consistent. The slight difference may be due to the error of the simulation and uncertainty of posterior distribution. The fraction of DM made up of PBHs could be constrained to  $\sim 0.1\% - 0.3\%$  for  $\geq 500 M_{\odot}$  at 68% confidence level. In addition to the null search of lensed GWs, we also assume the situation ( $\beta_{\text{PBH}} = 0$ ) that a BBH source with redshift  $z_s = 2$  is lensed by a PBH with the redshifted lens mass of  $300 M_{\odot}$ . In this case, the lens mass would be in the range of  $[100 M_{\odot}, 300 M_{\odot}]$ . As shown in the Figure 6, we can obtain 68% confidence level of the  $f_{\text{PBH}}$  from the posterior distribution at this mass range. The constraints on  $f_{\text{PBH}}$  are  $0.105^{+0.147}_{-0.064}$  with  $100 M_{\odot}$ ,  $0.064^{+0.083}_{-0.039}$  with  $200 M_{\odot}$  and  $0.057^{+0.071}_{-0.034}$  with  $300 M_{\odot}$  at 68% confidence level. Therefore if the lens mass is uniformly distributes in  $[100 M_{\odot}, 300 M_{\odot}]$ , the constraints on the  $f_{\text{PBH}}$  can be between 2.3% and 25.2%.

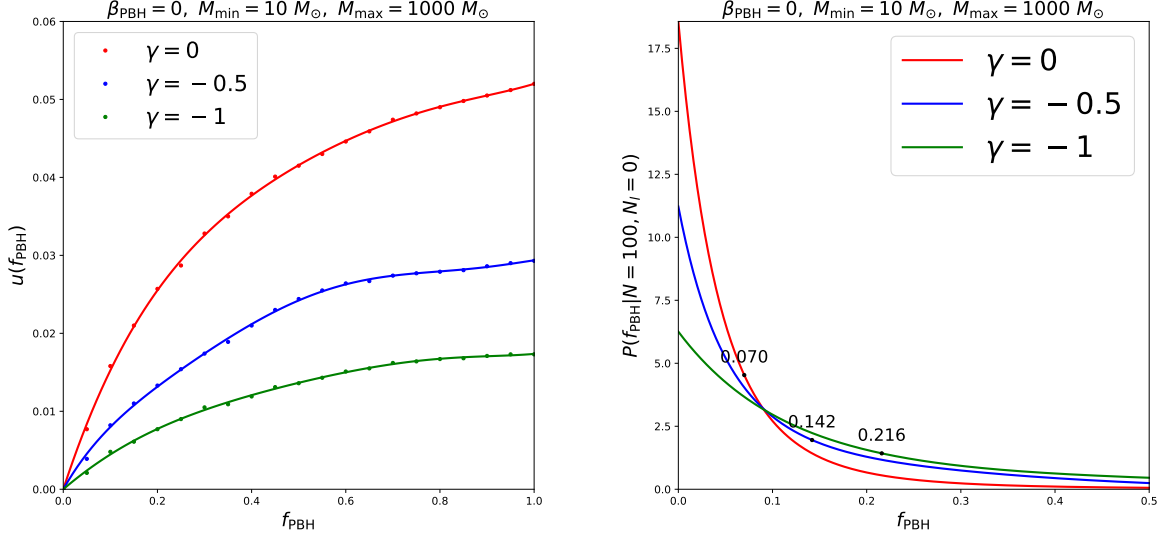


**Figure 7.** The same as Figure 3, left panel shows the fraction of simulated events with a power law mass function for lens. Right panel shows posteriors with 68% confidence level. Curves with different color correspond to results with different power exponent  $\gamma = -1, -0.5, 0$ .

For extended mass distribution of lens mass, we assume a power-law mass function with different power exponent  $\gamma = -1, -0.5, 0$ . In order to distinguish the mass distribution in the PBH binaries as GW sources, we just analyze the results for  $\beta_{\text{PBH}} = 0$ . Then the fraction of simulated events and the posterior of  $f_{\text{PBH}}$  assuming 100 detected BBH events with null lensed search are shown in Figure 7. In this model, the  $\gamma = 0$  case corresponds to a flatter mass distribution, which leads more lens of larger mass to contribute lensed probability and stronger limits. Comparing with the results from first plot of Figure 4, we find that the equivalent mass for the power-law mass function with  $\gamma = 0$  is approximately equal to  $100 M_{\odot}$ .

## 5 CONCLUSION

In this paper, we have derived constraints on the  $f_{\text{PBH}}$  at mass range  $\geq 50 M_{\odot}$  by assuming two representative scenarios of GW sources. First, we apply the method of Bayesian analysis for the third-generation detector i.e. the Cosmic Explorer, to derive constraints on the abundance of PBH,  $f_{\text{PBH}}$ . We obtain that it can be constrained to  $\leq 0.1\%$  for  $\geq 500 M_{\odot}$  at 68% confidence level from 100 unlensed GW events of BBH. This result can be compared with other observational limitations in the future, such as lensing effect of FRB (Zhou et al. 2022a). In addition, we assume that a GW events happened at redshift  $z_s = 2$  in 100 observed BBH events is lensed by a PBH with the redshifted lens mass being  $300 M_{\odot}$ , which can constrain  $f_{\text{PBH}}$  to 2.3% – 25.2%. If one lensed signal is identified from 1000 GW events, the constraint on  $f_{\text{PBH}}$  will be enhanced by an order of magnitude. In addition to the above constraints on the abundance of PBHs in the framework of monochromatic mass distribution of lens, we also consider a test extended mass distribution of lens to get more general constraints of  $f_{\text{PBH}}$ . After deducing the equivalent mass for a given input of extended mass distribution, we can

then read off the  $f_{\text{PBH}}$  for that distribution by using Figure 4 and Figure 7. It should be noted that our analysis neglects the macrolensing effect from the structures in hosting galaxy (Diego 2020; Cheung et al. 2021). Besides, possible astrophysical microlens in hosting galaxies may contaminate the constraints on the abundance of PBH (Christian et al. 2018).

Constraints on the  $f_{\text{PBH}}$  will be significantly improved because of the rapid increase of the number of GWs detected by various surveys and increased horizon distance of the next generation GW detectors in the near future. As a result, there would be significant overlap between the areas constrained from GW detection and the one from other electromagnetic observations. Then, it will be possible to jointly constrain the abundance and mass distribution of PBHs by combining these two kinds of promising multi-messenger observations. It is foreseen that these joint constraints will be of great importance for exploring the nature of PBHs or even their formation mechanisms relating to the physics of the early universe.

## ACKNOWLEDGEMENTS

This work was supported by the National SKA Program of China No. 2020SKA0110402; National key R&D Program of China (Grant No. 2020YFC2201600); National Key Research and Development Program of China Grant No. 2021YFC2203001; National Natural Science Foundation of China under Grants Nos. 11920101003, 11722324, 11603003, 11633001, 12073088, and U1831122; Guangdong Major Project of Basic and Applied Basic Research (Grant No. 2019B030302001), the Strategic Priority Research Program of the Chinese Academy of Sciences, Grant No. XDB23040100, and the Interdiscipline Research Funds of Beijing Normal University.

**DATA AVAILABILITY**

The data underlying this article will be shared on reasonable request to the corresponding author.

**REFERENCES**

- Abbott, B. P., Abbott, R., Abbott, T. D., et al., 2016, *Phys.Rev.Lett.*, 116, 061102
- Abbott, B. P., et al., 2017, *Astrophys. J. Lett.*, 848, L13
- Aghanim, N., Akrami, Y., Ashdown, M., et al., 2020, *Astron. Astrophys.*, 641, A6
- Alcock, C., Allsman, R. A., Alves, D. R., et al., 2001, *Astrophys. J.*, 550, L169
- Ali-Haïmoud Y., Kovetz, E. D., Kamionkowski M., 2017, *Phys.Rev.D.*, 96, 123523
- Amaro-Seoane P., et al., 2017, arXiv:1702.00786
- Basak, S., Ganguly, A., Haris, K., Kapadia, S., Mehta, A. K., Ajith, P., 2022, *Astrophys. J. Lett.*, 926, L28
- Carr, B., Kohri, K., Sendouda, Y., Yokoyama, J., 2021, *Rept. Prog. Phys.*, 84, 116902
- Chen, Z.-C., Huang, Q.-G., 2018, *Astrophys. J.*, 864, 61
- Chen, Z.-C., Huang, F., Huang, Q.-G., 2019, *Astrophys. J.*, 871, 97
- Cheung, M. H. Y., Gais, J., Hannuksela, O. A., Li, T. G. F., 2021, *Mon. Not. Roy. Astron. Soc.*, 503, 3326
- Christian, P., Vitale, S., Loeb, A., 2018, *Phys.Rev.D.*, 98, 103022
- De Luca, V., Franciolini, G., Pani, P., Riotto, A., 2020, *J. Cosmol. Astropart.Phys.*, 2020, 044
- Diego, J. M., 2020, *Phys.Rev.D.*, 101, 123512
- Dvorkin, L., Vangioni, E., Silk, J., Uzan, J.-P., Olive, K. A., 2016, *Mon. Not. Roy. Astron. Soc.*, 461, 3877
- Feeney S. M., Peiris H. V., Nissanke S. M., Mortlock D. J., 2021, *Phys. Rev. Lett.*, 126, 171102
- Finn, L. S., 1996, *Phys.Rev.D.*, 53, 2878
- Green, A. M., 2016, *Phys.Rev.D.*, 94, 063530
- Green, A. M., Kavanagh, B. J., 2021, *J.Phys.G*, 48, 043001
- Griest, K., Cieplak, A. M., Lehner, M. J., 2013, *Phys.Rev.Lett.*, 111, 181302
- Hotokezaka, K., Nakar, E., Gottlieb, O., Nissanke, S., Masuda, K., Hallinan, G., Mooley, K. P., Deller, A. T., 2019, *Nature Astron.*, 3, 940
- Hu W.-R., Wu Y.-L., 2017, *National Science Review*, 4, 685
- Hütsi, G., Raidal, M., Vaskonen, V., Veermäe, H., 2021, *J. Cosmol. Astropart.Phys.*, 2021, 068
- Ji, L.-Y., Kovetz, E. D., Kamionkowski, M., 2018, *Phys.Rev.D.*, 98, 123523
- Jung S., Shin C. S., 2019, *Phys. Rev. Lett.*, 122, 041103
- Kannike, K., Marzola, L., Raidal, M., Veermäe, H., 2017, *J. Cosmol. Astropart.Phys.*, 09, 020
- Kassiola, A., Kovner, I., Blandford, B. D., 1991, *Astrophys. J.*, 381, 6
- Kawamura, S., et al., 2019, *Int. J. Mod. Phys. D.*, 28, 1845001
- Laha, R., Muñoz, J. B., Slatyer, T. R., 2020, *Phys.Rev.D.*, 101, 123514
- Liao K., Tian S., Ding X., 2020a, *Mon. Not. Roy. Astron. Soc.*, 495, 2002
- Liao, K., Zhang, S.-B., Li, Z., Gao, H., 2020b, *Astrophys. J. Lett.*, 896, L11
- Lin, S.-J., Li, A., Gao, H., et al., 2022, *Astrophys. J.*, 931, 1
- Luo J., et al., 2016, *Class.Quant.Grav.*, 33, 035010
- Muñoz, J. B., Kovetz E. D., Dai L., Kamionkowski M., 2016, *Phys.Rev.Lett.*, 117, 091301
- Ng Ken, K. Y., Franciolini, G., Berti, E., Pani, P., Riotto, A., Vitale, S., 2022, arxiv: 2204.11864
- Niikura, H., Masahiro, T., Naoki, Y., et al., 2019a, *Nature Astronomy*, 3, 524.
- Niikura, H., Takada, M., Yokoyama, S., Sumi, T., Masaki, S., 2019b, *Phys.Rev.D.*, 99, 083503
- Raidal, M., Vaskonen, V., Veermäe, H., 2017, *J. Cosmol. Astropart.Phys.*, 09, 037
- Raidal, M., Vaskonen, V., Veermäe, H., 2018, *J. Cosmol. Astropart.Phys.*, 02, 018
- Reitze, D., et al., 2019, *Bull. Am. Astron. Soc.*, 51, 035
- Sasaki, M., Suyama, T., Tanaka, T., Yokoyama, S., 2016, *Phys. Rev. Lett.*, 117, 061101
- Sasaki, M., Suyama, T., Tanaka, T., Yokoyama, S., 2018, *Class.Quant.Grav.*, 35, 063001
- Takahashi, R., Nakamura, T., 2003, *Astrophys. J.*, 595, 1039
- Tisserand, P., Guillou, P., Afonso, C., et al., 2007, *Astron. Astrophys.*, 469, 387
- Urrutia, J., Vaskonen, V., 2021, *Mon. Not. Roy. Astron. Soc.*, 509, 1358
- Vangioni, E., Olive, K. A., Prestegard, T., Silk, J., Petitjean, P., Mandic, V., 2015, *Mon. Not. Roy. Astron. Soc.*, 447, 2575
- Wang, J.-S., Herrera-Martín, A., Hu, Y.-M., 2021, *Phys.Rev.D.*, 104, 083515
- Wilkinson, P. N., Henstock, D. R., Browne, W. A., et al., 2001, *Phys.Rev.Lett.*, 86, 584
- Wong, K. W. K., Franciolini, G., De Luca, V., Baibhav, V., Berti, E., Pani, P., Riotto, A., 2021, *Phys.Rev.D.*, 103, 023026
- Wu, Y., 2020, *Phys.Rev.D.*, 101, 083008
- Yoshida, Soda, D., J., 2018, *Int. J. Mod. Phys. D.*, 27, 1850096
- Zhou, H., Li, Z.-X., Huang, Z.-Q., Gao, H., Huang, L., 2022a, *Mon. Not. Roy. Astron. Soc.*, 511, 1141
- Zhou, H., Li, Z.-X., Liao, K., Niu, C.-H., Gao, H., Huang, Z.-Q., Huang, L., Zhang, B., 2022b, *Astrophys. J.*, 928, 124
- Zhou, H., Lian, Y.-J., Li, Z.-X., Cao, S., Huang, Z.-Q., 2022c, *Mon. Not. Roy. Astron. Soc.*, 513, 3627